FERMILAB-PUB-10-362-A

CoGeNT, DAMA, and Neutralino Dark Matter in the Next-To-Minimal Supersymmetric Standard Model

John F. Gunion[1], Alexander V. Belikov[2], and Dan Hooper[3,4]
[1] *Department of Physics, University of California, Davis, CA 95616*
[2] *Department of Physics, The University of Chicago, Chicago, IL 60637*
[3] *Center For Particle Astrophysics, Fermi National Accelerator Laboratory, Batavia, IL 60510*
[4] *Department of Astronomy and Astrophysics, University of Chicago, Chicago, IL 60637*

We assess the extent to which the NMSSM can allow for light dark matter in the 2 GeV $\lesssim m_{\widetilde{\chi}_1^0} \lesssim$ 12 GeV mass range with correct relic density and large spin-independent direct-detection cross section, σ_{SI}, in the range suggested by CoGeNT and DAMA. For standard assumptions regarding nucleon s-quark content and cosmological relic density, ρ, we find that the NMSSM falls short by a factor of about 10 to 15 (3 to 5) without (with) significant violation of the current $(g-2)_\mu$ constraints.

PACS numbers: 95.35.+d, 12.60.Jv, 14.80.Da; UCD-HEP-TH-2010-13; FERMILAB-PUB-10-362-A

arXiv:1009.2555v1 [hep-ph] 14 Sep 2010

I. INTRODUCTION

The CoGeNT collaboration has announced detection of very low energy events which are not consistent with any known backgrounds [1]. One possible interpretation of these events is elastic scattering of a light dark matter particle ($m \sim 5-10$ GeV) with a spin-independent cross section, σ_{SI}, on the order of 2×10^{-40} cm^2 (*i.e.* 2×10^{-4} pb) [1–4]. This is not very far from the region required to explain the annual modulation observed by the DAMA/LIBRA collaboration [5]. A consistent interpretation of both the DAMA and CoGeNT observations [6] is for dark matter to have mass and cross section in a 2σ ellipse ranging from $\sigma_{SI} \sim 3\times10^{-4}$ pb at $m \sim 6$ GeV down to $\sigma_{SI} \sim 1.4\times10^{-4}$ pb at $m \sim 9$ GeV. Clearly, it is of great interest to explore different kinds of dark matter models with regard to their ability to yield large σ_{SI} for $m \sim 6-9$ GeV.

A number of groups have addressed this issue within the context of the minimal supersymmetric standard model (MSSM) [7, 8]. However, given the structure of the MSSM Higgs sector and constraints thereon from LEP and elsewhere, achieving the above cross section at low LSP mass is not possible [8, 9]. A much higher local density of dark matter than the measured cosmological dark matter density, $\rho = 0.3$ GeV/cm^3, would be needed to bring the σ_{SI} required to describe the CoGeNT/DAMA events down to the level possible within the MSSM. Basically, the problem is that the Higgs with Enhanced coupling to down quarks, whose exchange is primarily responsible for the elastic scattering of the LSP (the lightest neutralino) on a nucleon, must be rather heavy in the MSSM context after imposing LEP constraints. Of course, a local density much larger than the cosmological average could be assumed so as to get the needed σ_{SI} at low m. However, there is a second problem. For low LSP mass, the MSSM simply does not allow sufficient early universe annihilation to yield the observed cosmological average relic density once Tevatron limits on $B(B_s \to \mu^+\mu^-)$ are imposed [8].

Thus, it is interesting to see if an extension of the MSSM could allow the relevant Higgs boson to have lower mass than allowed in the MSSM, thereby achieving $\sigma_{SI} = (1.4-3.5)\times10^{-4}$ pb, while maintaining consistency with all constraints. In a previous paper [10], we explored this question within the context of supersymmetric models with an additional generic chiral singlet superfield and found that this was indeed possible, the successful scenarios being ones in which both the LSP and exchanged Higgs are substantially singlet in nature. In this paper, we focus on the concrete (and more restrictive) case of the next-to-minimal supersymmetric standard model (NMSSM). Our conclusion will be that the observed cosmological relic density can be achieved while maintaining consistency with limits on $B(B_s \to \mu^+\mu^-)$ but that the largest σ_{SI} values that can be achieved for standard inputs regarding the s-quark content of the nucleon fall short of the preferred σ_{SI} region of [6] by a significant factor. In particular, in the strict NMSSM, scenarios with a light singlet $\widetilde{\chi}_1^0$ and largely singlet light Higgs cannot be realized at high $\tan\beta$ while satisfying all other constraints. We also briefly discuss possibilities for enhancing the NMSSM cross sections by enhancing the s-quark nucleon content or reducing the required σ_{SI} using the recently proposed larger local density $\rho \sim [0.4-0.485]$ GeV/cm^3 (see [11] for a summary).

The remainder of this paper is structured as follows. In Sec. II, we outline the problems faced in the MSSM. In Sec. III, we discuss how the NMSSM can potentially avoid these problems without violating the relevant collider constraints. In Sec. IV, we turn to a detailed discussion of the NMSSM, including the point searching procedures we will employ and the constraints that must be obeyed. In Sec. V, we present the NMSSM benchmark points we have found with large σ_{SI} that satisfy all LEP and BaBar limits. We then examine implications of various additional constraints from the Tevatron, B physics and $(g-2)_\mu$ for such points. We discuss some phenomenological issues for

Operated by Fermi Research Alliance, LLC under Contract No. De-AC02-07CH11359 with the United States Department of Energy.

those points that survive all constraints. In Sec. VI, we summarize our results and draw conclusions.

II. LIGHT NEUTRALINOS IN THE MSSM

In the MSSM, there are two CP-even Higgs bosons, the h^0 and the H^0 with $m_{h^0} < m_{H^0}$. In the usual convention, one writes $H^0 = \cos\alpha H_d + \sin\alpha H_u$, $h^0 = -\sin\alpha H_d + \cos\alpha H_u$, where $H_{d,u}$ are the neutral Higgs fields that couple to down and up type quarks respectively. An especially crucial parameter of the model is $\tan\beta \equiv \langle H_u\rangle/\langle H_d\rangle$. Relative to the SM Higgs, $g_{h^0VV} = \sin(\beta-\alpha)$ and $g_{H^0VV} = \cos(\beta-\alpha)$, where $VV = W^+W^-$ or ZZ. The structure of the model combined with LEP constraints require that $m_{h^0}, m_{H^0} > 90-100$ GeV. In this case, $\cos(\beta-\alpha)$ must be fairly small, especially at large $\tan\beta$. The combination of large $\tan\beta$ and small $\cos(\beta-\alpha)$ implies $\alpha \sim 0$ and $\cos\alpha \sim 1$. In this situation, the only way to get a large spin-independent cross section for lightest neutralino, $\widetilde{\chi}_1^0$, scattering on the nucleon is via exchange of the H^0 between the $\widetilde{\chi}_1^0$ ($g_{H^0\widetilde{\chi}_1^0\widetilde{\chi}_1^0} \propto \cos\alpha$) and the down type quarks contained in the nucleon ($g_{H^0dd,ss,bb} \propto \tan\beta\cos\alpha$). A rough formula for the spin-independent cross section was obtained in [10]:

$$\sigma_{SI} \;\approx\; 1.7\times 10^{-5}\ \text{pb}\left(\frac{N_{13}^2}{0.1}\right)\left(\frac{\tan\beta}{50}\right)^2\left(\frac{100\text{GeV}}{m_{H^0}}\right)^4\cos^4\alpha\,, \tag{1}$$

where we have written $\widetilde{\chi}_1^0 = N_{11}\widetilde{B} + N_{12}\widetilde{W}^3 + N_{13}\widetilde{H}_d + N_{14}\widetilde{H}_u$. In the above, N_{13}^2 cannot be much larger than 0.1 because of limits on the Z invisible width. Given that LEP constraints basically force $m_{H^0} \gtrsim 100$ GeV and that other constraints (including b-quark Yukawa perturbativity) are very difficult to satisfy for $\tan\beta \geq 50$, we see that the MSSM is unable to obey all constraints and yield σ_{SI} larger than a fraction of 10^{-4} pb.

In addition, one must consider whether the MSSM allows for sufficient early-universe annihilation to achieve $\Omega_{\widetilde{\chi}_1^0}h^2 < 0.1$. To briefly review, the density of neutralino dark matter in the universe today can be determined by the particle's annihilation cross section and mass. In the mass range we are considering here, the dominant annihilation channel is to $b\bar{b}$ (or to a lesser extent to $\tau^+\tau^-$) through the s-channel exchange of the pseudoscalar Higgs boson, A. The thermally averaged cross sections for these processes are given by

$$\begin{aligned}\langle\sigma_{\widetilde{\chi}_1^0\widetilde{\chi}_1^0\to A\to b\bar{b},\tau^+\tau^-}\,v\rangle \;&=\; \frac{(3,1)g_2^2 m_{b,\tau}^2\tan^2\beta}{8\pi m_W^2}\,\frac{m_{\widetilde{\chi}_1^0}^2\sqrt{1-m_{b,\tau}^2/m_{\widetilde{\chi}_1^0}^2}}{(4m_{\widetilde{\chi}_1^0}^2-m_{A^0}^2)^2+m_A^2\Gamma_{A^0}^2}\\ &\times\;[(N_{13}\sin\beta - N_{14}\cos\beta)(g_2N_{12}-g_1N_{11})]^2,\end{aligned} \tag{2}$$

where Γ_{A^0} is the width of the pseudoscalar MSSM Higgs. And although there are additional contributions from scalar Higgs exchange, these are suppressed by the square of the relative velocity of the neutralinos, and thus are substantially suppressed in the process of thermal freeze-out.

The thermal relic abundance of neutralinos is given by

$$\Omega_{\widetilde{\chi}_1^0}h^2 \approx \frac{10^9}{M_{\text{Pl}}}\frac{m_{\widetilde{\chi}_1^0}}{T_{\text{FO}}\sqrt{g_\star}}\frac{1}{\langle\sigma_{\widetilde{\chi}_1^0\widetilde{\chi}_1^0}v\rangle} \tag{3}$$

where $g_\star$ is the number of relativistic degrees of freedom available at freeze-out and T_{FO} is the temperature at which freeze-out occurs:

$$\frac{m_{\widetilde{\chi}_1^0}}{T_{\text{FO}}} \approx \ln\left(\sqrt{\frac{45}{8}}\frac{m_{\widetilde{\chi}_1^0}M_{\text{Pl}}\langle\sigma_{\widetilde{\chi}_1^0\widetilde{\chi}_1^0}v\rangle}{\pi^3\sqrt{g_\star m_{\widetilde{\chi}_1^0}/T_{\text{FO}}}}\right). \tag{4}$$

For the range of masses considered here, and for cross sections which will yield approximately the measured dark matter abundance, we find $m_{\widetilde{\chi}_1^0}/T_{\text{FO}} \approx 20$.

For $m_{\widetilde{\chi}_1^0} \sim 5-15$ GeV, the relic abundance of MSSM neutralinos is then approximately given by

$$\Omega_{\widetilde{\chi}_1^0}h^2 \approx 0.1\left(\frac{0.1}{N_{13}^2}\right)\left(\frac{50}{\tan\beta}\right)^2\left(\frac{m_{A^0}}{100\,\text{GeV}}\right)^4\left(\frac{9\,\text{GeV}}{m_{\widetilde{\chi}_1^0}}\right)^2. \tag{5}$$

Given that LEP limits require $m_{A^0} \gtrsim 90-100$ GeV and that $\tan\beta$ as large as 50 is already in the non-perturbative domain for the b-quark coupling, it requires a very extreme choice of parameters to get the measured dark matter density of our universe to be as small as that measured, $\Omega_{\text{CDM}}h^2 = 0.1131 \pm 0.0042$ [12]. And, even with such

extreme parameter choices, σ_{SI} can be no larger than $\sim 1.7 \times 10^{-5}$ pb. Of course, it is true that the same extreme choice of parameters that minimizes $\Omega_{\tilde{\chi}_1^0} h^2$, bringing it close to the observed value, at the same time maximizes σ_{SI}. However, there is a further barrier to achieving the minimal $\Omega_{\tilde{\chi}_1^0} h^2$, maximal σ_{SI} scenario. In particular, the above discussion does not yet include consideration of the Tevatron limits on $B(B_s \to \mu^+\mu^-)$. In [8] (see their Fig. 3b), it was found that the MSSM simply cannot give the correct relic density for $m_{\tilde{\chi}_1^0}$ in the CoGeNT/DAMA region once the $B(B_s \to \mu^+\mu^-)$ limit is imposed in addition to the LEP limits. This situation motivates us to consider supersymmetric scenarios beyond the MSSM. In the next section, we will demonstrate that in the NMSSM it is possible to alleviate both the elastic scattering cross section and relic abundance problems found in the MSSM.

III. THE NMSSM

In the NMSSM, one adds exactly one singlet chiral superfield to the MSSM. As is well known, this allows a completely natural explanation for the size of the μ term [13] and can reduce electroweak fine-tuning [14], and potentially catalyze electroweak baryogenesis [15]. The NMSSM superpotential is given by

$$\lambda \hat{S} \hat{H}_u \hat{H}_d + \tfrac{1}{3}\kappa \hat{S}^3 \ , \tag{6}$$

and the associated part of the soft Lagrangian is given by

$$\lambda A_\lambda S H_u H_d + \tfrac{1}{3}\kappa A_\kappa S^3 + H.c. \tag{7}$$

The restriction to the forms given above is implemented by invoking a Z_3 symmetry to remove all other possible terms. In particular, only the dimensionless λ and κ superpotential terms are allowed. All dimensionful parameters are generated by soft-SUSY-breaking. An effective μ value is automatically obtained as $\mu_{\rm eff} = \lambda \langle S \rangle$. This very attractive extension of the MSSM allows for a considerable expansion of the phenomenological possibilities. In particular, the singlet superfield leads to five neutralinos, three CP-even Higgs bosons ($h_{1,2,3}$) and two CP-odd Higgs bosons ($a_{1,2}$). In general, the neutralino mass eigenstates are mixtures of the MSSM neutralino fields and the singlino field that is part of the singlet superfield; the CP-even (odd) Higgs mass eigenstates are similarly mixtures of the CP-even (odd) MSSM fields and the CP-even (odd) components of the complex singlet scalar component of the singlet superfield.

Within the NMSSM, it is very natural for the lightest pseudoscalar Higgs, a_1, to have low mass (see [16]). In particular, $U(1)_R$ or $U(1)_{\rm PQ}$ symmetries can appear which lead to values of m_{a_1} well below the electroweak scale. If one is close to either symmetry limit, the a_1 will be at least moderately singlet-like (as opposed to being more purely MSSM-Higgs-like) and will likely be beyond the reach of current collider constraints.

That a light a_1 in the NMSSM can allow a very light dark matter particle in the CoGeNT mass region with correct relic density was established in [17]. This is because the light a_1 s-channel annihilation process is typically fairly close to being 'on-pole', $2m_{\tilde{\chi}_1^0} \sim m_{a_1}$, as opposed to $2m_{\tilde{\chi}_1^0} \ll m_{A^0}$ for the rather heavy A^0 of the MSSM. However, in the scans performed in [17] we did not encounter points with cross sections as large as those needed to describe the tentative CoGeNT/DAMA signal. We now describe a strategy for getting the largest possible cross section.

To enhance the neutralino's elastic scattering cross section, we need a Higgs mass eigenstate that is primarily H_d (so that it will have enhanced couplings to down-type quarks at large $\tan\beta$) with mass lower than possible for the H^0 of the MSSM. While this is not as easy to arrange in the NMSSM as are low values of the lightest CP-odd Higgs mass, it is still possible. The value of the down-type diagonal term of the NMSSM scalar Higgs (squared) mass matrix at tree-level is given by

$$m^2_{H,22} = \frac{g^2 v^2}{1+\tan^2\beta} + \mu \tan\beta (A_\lambda + \kappa\mu/\lambda), \tag{8}$$

where v is the Standard Model Higgs vacuum expectation value. At large $\tan\beta$, in order for this to fall significantly below the value of the up-type Higgs entry (which is generally $m^2_{H,11} \approx (85{\rm GeV})^2$), there must be some cancellation between the A_λ and $\kappa\mu/\lambda$ terms. This cancellation also suppresses the mixing term between up-type and down-type scalar Higgs bosons. The down-type mass can further be protected from large radiative corrections if the two stop masses are similar. Together, these features can potentially lead to a down-type scalar Higgs boson with a mass significantly below 100 GeV.

The scenarios that can potentially lead to large σ_{SI} are then ones in which the lightest of the NMSSM Higgs bosons, the h_1, is not SM-like, has enhanced coupling to down-type quarks and has mass below $\sim$ 100 GeV. The h_2 will typically be SM-like and for m_{h_1} below 100 GeV is typically not very heavy – $m_{h_2} \gtrsim 110$ GeV for $m_{\rm SUSY} = 500$ GeV and $m_{h_2} \gtrsim 115$ GeV for $m_{\rm SUSY} = 1$ TeV. LEP limits will be very constraining in this situation. In addition,

many B-physics constraints will enter as will constraints from $(g-2)_\mu$. Also important will be limits on $b\bar{b}+Higgs$ production with $Higgs \to \tau^+\tau^-$ and $t \to h^+ b$ decays with $h^+ \to \tau^+\nu_\tau$. We will employ augmented versions of NMHDECAY [18, 19] supplemented by micrOMEGAs [20] (the latter will be implemented as in NMSSMTools [21]) for our exploration of the NMSSM parameter space.

IV. CONSTRAINTS AND SCANNING IN THE NMSSM

As noted, we have performed our scanning using an augmented version of NMHDECAY linked to micrOMEGAs as in NMSSMTools. NMHDECAY currently incorporates all LEP limits on Higgs bosons as well as LEP limits on neutralinos and charginos.[1] We have augmented NMHDECAY to include the recent ALEPH constraints [23] on $e^+e^- \to Z + Higgs$ with $Higgs \to aa$ (in our case $a = a_1$, the lightest CP-odd Higgs boson of the NMSSM) with $a \to \tau^+\tau^-$. Further, we have augmented NMHDECAY to include the combined CDF+D0 Tevatron constraints [24] on $b\bar{b} + Higgs$ production with $Higgs \to \tau^+\tau^-$ (for the scans performed in this paper, it is constraints in the case of $Higgs = h_1$ or a_2 that are typically relevant). [2] Finally, in the scenarios with large σ_{SI} the h^+ is inevitably light enough that $t \to h^+ b$ decays will be present and, since $\tan\beta$ is large, $h^+ \to \tau^+\nu_\tau$ will be completely dominant. We have thus augmented NMHDECAY to include the current D0 limits [25] on $B(t \to h^+ b) \times B(h^+ \to \tau^+\nu_\tau)$.[3] NMHDECAY also includes analysis of a large selection of B physics constraints. For our purposes, the most important ones turn out to be $B_s \to \mu^+\mu^-$, $B^+ \to \tau^+\nu_\tau$, and $b \to s\gamma$. We have also augmented NMHDECAY to incorporate full BaBar constraints on $\Upsilon_{nS} \to \gamma a$ with $a \to \mu^+\mu^-$ or $a \to \tau^+\tau^-$ as implemented in [26]. Finally, we have examined the NMHDECAY predictions for $(g-2)_\mu$ for high-σ_{SI} cases. In our search for desirable points, we have demanded that all the LEP limits, including the ALEPH limits, are strictly obeyed. We have also demanded that the BaBar limits be strictly satisfied.

The $b\bar{b}+Higgs(\to \tau^+\tau^-)$ and $t \to h^+(\to \tau^+\nu)b$ limits are treated somewhat differently. In the experimental papers, the observed limits are plotted as a function of the relevant Higgs mass in comparison to the expected limits. The expected limits have error bars that are partly statistical and partly systematic (including theory systematics) that have been combined in quadrature, *i.e.* assuming a Gaussian distribution in particular for theoretical systematics. We believe that treating the observed limits in these cases as true limits is somewhat dubious. In our opinion, it would be much better to have separated the statistical errors from the systematic errors and ask what band about the observed limits would result from pushing all systematics in the least or most favorable direction. In the absence of sufficient information to carry out this task, we will simply assess the impact of relaxing the observed limits in the above channels by an amount equivalent to the 1σ or 2σ error bands (as plotted relative to the expected limits) relative to the observed limits.[4]

In assessing the $B^+ \to \tau^+\nu_\tau$, $b \to s\gamma$ and $(g-2)_\mu$ constraints contained in the basic NMHDECAY program ($B_s \to \mu^+\mu^-$ is handled differently as described later) we have adopted the following procedure. The NMHDECAY output gives the model point prediction as well as the maximum and minimum values after adding and subtracting the theoretical error. Let us call these P_0, P_+ and P_-, respectively. Also contained in the output is the $\pm 2\sigma$ interval for the experimentally observed value or limit, which we label as $O_{+2\sigma}$ and $O_{-2\sigma}$, respectively. Any point for which P_+ or P_- falls within the interval $I = [O_{-2\sigma}, O_{+2\sigma}]$ is deemed acceptable. If this is not the case we assess the extent of the violation of the constraint as follows. Let us say $P_- > O_{+2\sigma}$. Define $\Delta = |P_- - O_{+2\sigma}|$. We then compute $R_\sigma = \Delta/E$, where E is a combined error associated with the experimental and theoretical errors: $E \equiv [(|O_{+2\sigma} - O_{-2\sigma}|/4)^2 + (|P_+ - P_-|/2)^2]^{1/2}$. If P_+ or P_- falls within the interval $I = [O_{-2\sigma}, O_{+2\sigma}]$ we set $R_\sigma = 0$. We will summarize the values found for R_σ for high-σ_{SI} points for each of the above three constraints.

In our scans, we have held fixed the soft scales $M_2 = 200$ GeV and $M_3 = 300$ GeV, allowing for varying values of M_1 (which essentially fixes the mass of the bino-like neutralino). Our scans have been performed for fixed values of $\mu_{\rm eff} = +200$ GeV and -200 GeV. (It seems that smaller $|\mu_{\rm eff}|$ values do not allow large σ_{SI} to be consistent with all other constraints. Conversely, larger $|\mu_{\rm eff}|$ tends to lower the achievable σ_{SI}.) We have considered three values of $\tan\beta$, $\tan\beta = 40$, $\tan\beta = 45$ (only for $\mu_{\rm eff} < 0$) and $\tan\beta = 50$. We have adopted a universal value of $m_{\rm SUSY}$ for all the soft SUSY-scale slepton and squark SUSY-breaking masses. We consider $m_{\rm SUSY} = 500$ GeV and 1 TeV. We have adopted a universal value for all the soft A parameters, *i.e.* $A_{soft} \equiv A_t = A_b = A_\tau, \ldots$. It turns out that essentially

---

[1] We have retained the stronger cross section constraints of the original NMHDECAY program rather than weakening them in the manner suggested in [22]. However, we have updated the limit on $\Gamma_{Z\to\tilde{\chi}_1^0\tilde{\chi}_1^0}$ to 1.9 MeV as in [22].

[2] Experimental plots assume the MSSM for which the H and A are nearly degenerate whereas in most NMSSM cases h_2 and a_2 are not degenerate, implying a somewhat weaker constraint on the separate $b\bar{b}h_2$ and $b\bar{b}a_2$ couplings.

[3] Limits in this channel from CDF are not currently available.

[4] In the $t \to h^+ b$ case, plots only show a 1σ error band. We have simply doubled this for an approximation to the 2σ error band.

the only way to obtain a value for $B(B_s \to \mu^+\mu^-)$ below the current experimental limit when $\tan\beta$ is large is to choose A_{soft} rather precisely (typically to within 1%). At high $\tan\beta$, it turns out that the appropriate choice for A_{soft} is essentially only a function of $m_{\rm SUSY}$. For each choice of $m_{\rm SUSY}$, we have determined the appropriate A_{soft} and have then held it fixed at this value as we scan over other parameters and assess all the other constraints (LEP, BaBar, Tevatron, ...).

In all our scans, we have consistently found that large σ_{SI} is only achieved if the $\widetilde{\chi}_1^0$ is mostly bino, implying that $m_{\widetilde{\chi}_1^0}$ is pretty much fixed to be close to M_1. As a result, we have performed scans at a variety of M_1 values in the general CoGeNT range. For any given M_1 we thus end up scanning in $\lambda, \kappa, A_\lambda, A_\kappa$, demanding, as sketched above, complete consistency with all LEP and BaBar limits, but allowing for some deviation from B-physics, Tevatron and $(g-2)_\mu$ nominal constraints. For a choice of $\lambda, \kappa, A_\lambda, A_\kappa$ that is allowed by LEP and BaBar constraints (at the given A_{soft}), there is no guarantee that $\Omega h^2 \sim 0.11$ will be obtained. Fortunately, it is often the case that one can adjust m_{a_1} (by changing A_κ by a relatively small amount) and or $m_{\widetilde{\chi}_1^0}$ (by changing M_1) so that $\Omega h^2 \sim 0.11$ (we accept points within the NMSSMTools-defined window, $0.094 \leq \Omega h^2 \leq 0.136$) is achieved without destroying consistency with LEP and BaBar limits. The results of these scans after this adjustment are presented in the following section.

V. BENCHMARK MODELS IN THE NMSSM

We begin with plots, Figs. 1 and 2, of σ_{SI} vs. $m_{\widetilde{\chi}_1^0}$ for $\mu_{\rm eff} = -200$ GeV and $\mu_{\rm eff} = +200$ GeV. We only give points found that have fairly large σ_{SI}. For these two figures, only the LEP constraints, BaBar constraints, $B(B_s \to \mu^+\mu^-)$ limits and $0.094 \leq \Omega h^2 \leq 0.136$ are required to be satisfied. We refer to these as level-I constraints. Many of the plotted points with the largest σ_{SI} values fail at some level one or more of the other constraints, as we shall describe.

For $\mu_{\rm eff} = -200$ GeV we see in Fig. 1 that fairly large values of σ_{SI} (only a factor of 3 to 5 or so below the values typical of the preferred CoGeNT/DAMA region) can be obtained. Such points typically have both large $\tan\beta = 50$ and low $m_{\rm SUSY}$ (so that m_{h_1} can be relatively smaller). In contrast, Fig. 2 shows that for $\mu_{\rm eff} = +200$ GeV we never found any points with $\tan\beta = 50$ and $m_{\rm SUSY} = 500$ GeV that were consistent with LEP and BaBar limits. Consistent points were found for $\tan\beta = 40$ and $m_{\rm SUSY} = 500$ GeV with $\sigma_{SI} \sim 0.1 \times 10^{-4}$ pb. For $m_{\rm SUSY} = 1$ TeV, consistent points are found for both $\tan\beta = 50$ and $\tan\beta = 40$ for which the largest cross sections found are of order 0.2×10^{-4} pb and 0.15×10^{-4} pb, respectively, both of which are significantly below the cross section needed to explain CoGeNT/DAMA events.

As anticipated from our earlier discussions, one finds that almost all the high-σ_{SI} points for either sign of $\mu_{\rm eff}$ have $C_V(h_1) \ll 1$ (where $C_V(h) = g_{hVV}/g_{h_{\rm SM}VV}$), implying that either h_2 or h_3 is the SM-like Higgs boson. This was not imposed, but simply came out of the scan when large σ_{SI} was required. This shows that our intuition as to how to achieve large σ_{SI} was correct. For many cases, $m_{h_2} < 110$ GeV and $C_V(h_2) \sim 1$. Such points escape LEP limits because $B(h_2 \to a_1 a_1)$ is large and 10 GeV $\lesssim m_{a_1} \lesssim 2m_B$, the 10 GeV lower bound so that BaBar constraints on $\Upsilon_{3S} \to \gamma a_1$ and ALEPH constraints on Zh_2 with $h_2 \to a_1 a_1 \to 4\tau$ are obeyed and the upper bound so that $a_1 \to b\bar{b}$ is forbidden.

Of interest for the following are the masses of the h_2 and h^+ for the large σ_{SI} points. These are shown in Figs. 3 and 4. One should take note of the rather low values of m_{h_1}, m_{h_2} and m_{h^+}. (For some points, m_{h_3} is also quite small.) Low m_{h^+} combined with large $\tan\beta$ implies that $B(t \to h^+ b)$ will be significant and that $B(h^+ \to \tau^+\nu_\tau) \sim 1$. Low masses for the neutral Higgs bosons coupled with the fact that at least several of them will have enhanced $b\bar{b}$ coupling when $\tan\beta$ is large implies that $b\bar{b} + Higgs$ with $Higgs \to \tau^+\tau^-$ will have a high rate at a hadron collider for several of the neutral Higgs. Thus, Tevatron constraints will often be of importance, and future LHC results could have a deciding impact.

Indeed, let us now add to the LEP and BaBar constraints the requirement that the Tevatron constraints on $b\bar{b} + Higgs$ and $t \to h^+ b$ be satisfied within 1σ as defined in the previous section. The plot of Fig. 5 shows that for $\mu_{\rm eff} = -200$ GeV the points with largest σ_{SI} (*i.e.* those with low $m_{\rm SUSY}$ and hence lower m_{h_1} and large $\tan\beta$) do not satisfy the additional Tevatron constraints. The maximal cross section allowed is $\sim 0.3 \times 10^{-4}$ pb, which is distinctly below the $\sigma_{SI} = (1.4 - 3.5) \times 10^{-4}$ pb of the CoGeNT/DAMA region.

For $\mu_{\rm eff} = +200$ GeV, the LEP and BaBar constraints had already eliminated such points and imposing the Tevatron constraints at the 1σ level eliminates only the single point of Fig. 2 with $m_{\widetilde{\chi}_1^0} \sim 2.4$ GeV and $\sigma_{SI} \sim 0.28 \times 10^{-4}$ pb.

If we require that the Tevatron observed limits apply with no allowance for error, we obtain the plots shown in Fig. 6. The maximum σ_{SI} for both $\mu_{\rm eff} = -200$ GeV and $\mu_{\rm eff} = +200$ GeV in the CoGeNT $m_{\widetilde{\chi}_1^0}$ region is of order 0.14×10^{-4} pb, a factor of $10 - 20$ below the $\sigma_{SI} = (1.4 - 3.5) \times 10^{-4}$ pb CoGeNT/DAMA region.

We now turn to the impact on these results of $B^+ \to \tau^+\nu_\tau$, $b \to s\gamma$ and $(g-2)_\mu$ constraints. To assess these impacts, we employ R_σ defined earlier, where R_σ is computed for each of the above three cases. For $\mu_{\rm eff} = -200$ GeV, non-zero values of R_σ only arise for $B^+ \to \tau^+\nu_\tau$ and $(g-2)_\mu$. $R_\sigma(B^+ \to \tau^+\nu_\tau)$ for the plotted points is typically

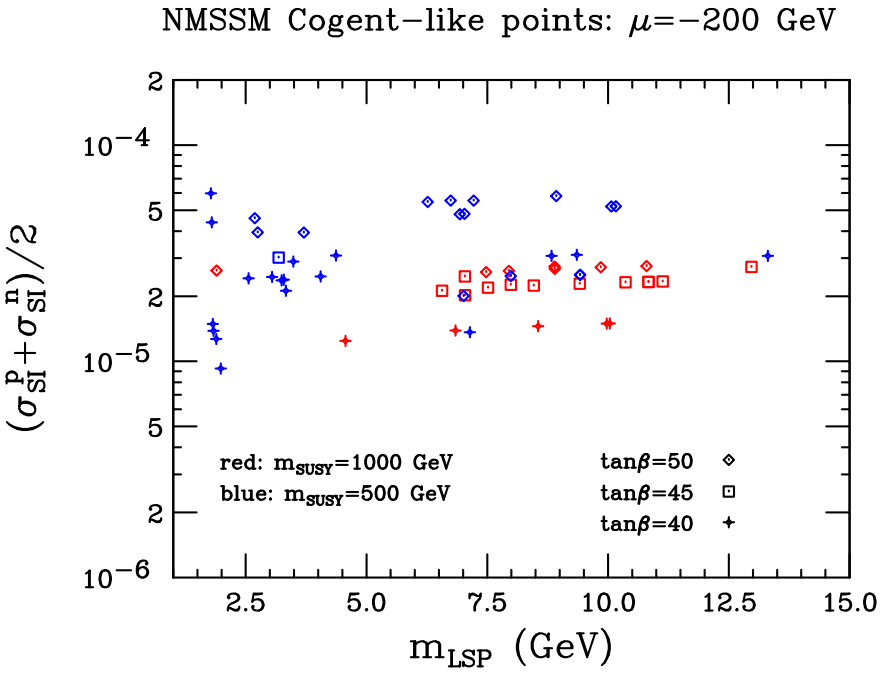

FIG. 1: σ_{SI} vs. $m_{\widetilde{\chi}_1^0}$ for $\mu_{\rm eff} = -200$ GeV. Parameters not shown are fixed as stated in the text. Only level-I constraints are imposed.

below, often well below, 0.4, which we do not regard as a significant exception to the experimental limits. On the other hand $R_\sigma((g-2)_\mu)$ is often quite large. Indeed, if we require $R_\sigma((g-2)_\mu) < 2$ then all points are eliminated except for those with very low $m_{\widetilde{\chi}_1^0} \sim 2.4$ GeV. Requiring $R_\sigma((g-2)_\mu) < 3$ leaves the points plotted in Fig. 7, *i.e.* it is the $m_{\rm SUSY} = 1000$ GeV points that can survive this very loose constraint. In short, if $(g-2)_\mu$ is taken seriously, the $\mu_{\rm eff} = -200$ GeV points must be eliminated from consideration. Of course, one should never completely rule out the possibility that significant additional new physics could contribute to $(g-2)_\mu$ without affecting the NMSSM structure of the Higgs and dark matter sectors.

In contrast, the vast majority of the $\mu_{\rm eff} = +200$ GeV points (and indeed all of those near the CoGeNT mass window) are fully consistent with both $B^+ \to \tau^+\nu_\tau$ and $(g-2)_\mu$ constraints within the NMHDECAY windows and only have small values of $R_\sigma(b \to s\gamma)$. For all of the plotted points in the $m_{\widetilde{\chi}_1^0} > 4$ GeV region, $R_\sigma(b \to s\gamma) \in [0.5, 0.6]$. Given the possibility of other new physics that might enter into $b \to s\gamma$ that might easily have no affect on the NMSSM Higgs and dark matter issues, we regard this as acceptable.

Let us focus on a few more details regarding the $\mu_{\rm eff} = +200$ GeV points. As already noted, only these are fully consistent with $(g-2)_\mu$ constraints. As described above, they have only a small violation of nominal $b \to s\gamma$ bounds. In the left-hand plot of Fig. 8, we show the range of m_{a_1} values as a function of $m_{\widetilde{\chi}_1^0}$. One observes the expected trend of increasing m_{a_1} with increasing $m_{\widetilde{\chi}_1^0}$ needed in order to achieve appropriate relic abundance.

As discussed in Ref. [27], scenarios with a light a_1 can potentially be probed by directly searching for the a_1 at hadron colliders. The discovery potential is basically a function of the strength of the $a_1 b\bar{b}$ reduced coupling, $C_{a_1 b\bar{b}}$. In the NMSSM context, $C_{a_1 b\bar{b}} = \cos\theta_A \tan\beta$, where $\cos\theta_A$ specifies the amount of the a_1 that resides in the MSSM-like doublet sector as opposed to the singlet component:

$$a_1 = \cos\theta_A a_{MSSM} + \sin\theta_A a_S \tag{9}$$

In the absence of $\cos\theta_A$ suppression, the a_1 would be strongly coupled to down-type quarks proportionally to $\tan\beta$.

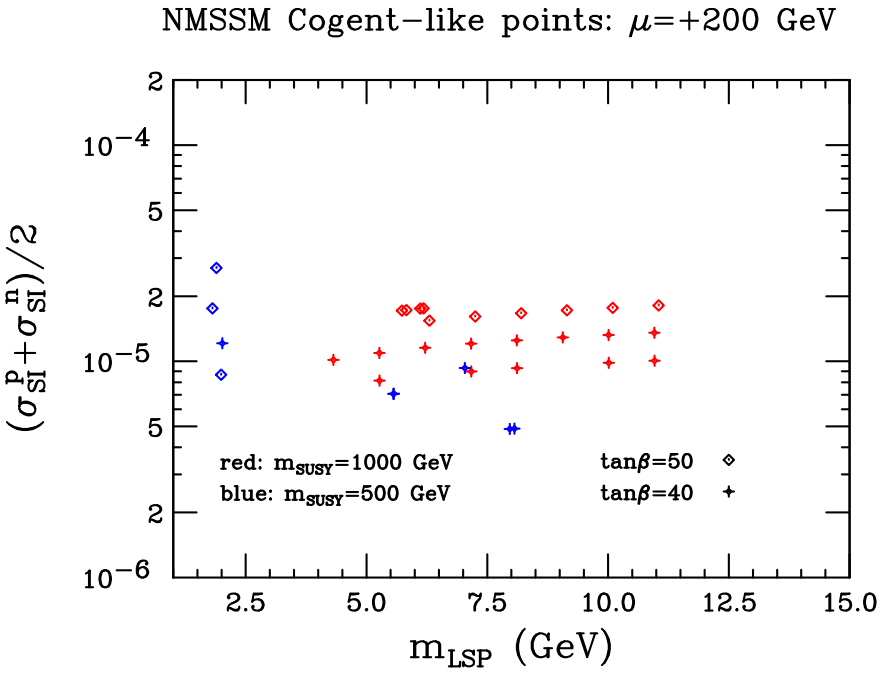

FIG. 2: σ_{SI} vs. $m_{\widetilde{\chi}_1^0}$ for $\mu_{\rm eff} = +200$ GeV. Parameters not shown are fixed as stated in the text. Only level-I constraints are imposed.

However, many of the points with large σ_{SI} have $\cos\theta_A$ values significantly below unity. The right-hand plot of Fig. 8 shows $|C_{a_1 b\bar{b}}|$ vs. m_{a_1} for all the $\mu_{\rm eff} = +200$ GeV points. We see significant variation of $|C_{a_1 b\bar{b}}|$, but find many points with fairly large values. Of course, the larger $|C_{a_1 b\bar{b}}|$ is, the easier it will be to detect the a_1 directly in hadronic collisions, for example via $b\bar{b}a_1$ production followed by $a_1 \to \tau^+\tau^-$ or $gg \to a_1 \to \mu^+\mu^-$. Some of the $|C_{a_1 b\bar{b}}|$ values are sufficiently large that early detection at the LHC might be feasible.

Another interesting question is how well the points plotted agree with precision electroweak constraints. This can be assessed by computing the effective precision electroweak mass defined by

$$\ln m_{eff} = \sum_{i=1,2,3} |C_V(h_i)|^2 \ln m_{h_i} \,. \tag{10}$$

One finds that all $\mu_{\rm eff} = +200$ GeV points with $m_{\rm SUSY} = 1$ TeV have $m_{eff} \in [114\ {\rm GeV}, 116\ {\rm GeV}]$. In comparison, the $m_{\rm SUSY} = 500$ GeV points can have m_{eff} as low as 100 GeV, thereby achieving excellent agreement with precision electroweak measurements. Such points are closely related to the "ideal" Higgs scenarios, but are more complex in nature. However, as shown in Fig. 2, the largest σ_{SI} that can be achieved for such points is of order 0.1×10^{-4} pb, a factor of $\gtrsim 15$ below that needed to most naturally describe the CoGeNT/DAMA observations.

Although we have not explicitly performed the necessary computations, we anticipate that the $m_{\rm SUSY} = 1000$ GeV points will have significant electroweak symmetry breaking (EWSB) finetuning (*i.e.* to predict the correct value of m_Z will require very precise adjustment of the GUT-scale soft-SUSY-breaking parameters) whereas much less finetuning should be required in the case of the $m_{\rm SUSY} = 500$ GeV points.

It is perhaps interesting to give details for the $\tan\beta = 40$, $m_{\rm SUSY} = 500$ GeV "semi-ideal-Higgs" point with $m_{\widetilde{\chi}_1^0}$ in the center of the CoGeNT mass region and $\sigma_{SI} \sim 0.1 \times 10^{-4}$ pb found in Fig. 2. The relevant details are presented in Table I. For this point it is the h_2 with $m_{h_2} \sim 97$ GeV that is mainly responsible for a substantial size for σ_{SI} (since $C_{h_2 b\bar{b}}$ is large — see the 3rd row of Table I). In contrast, the h_1 has relatively small down-type quark coupling as can

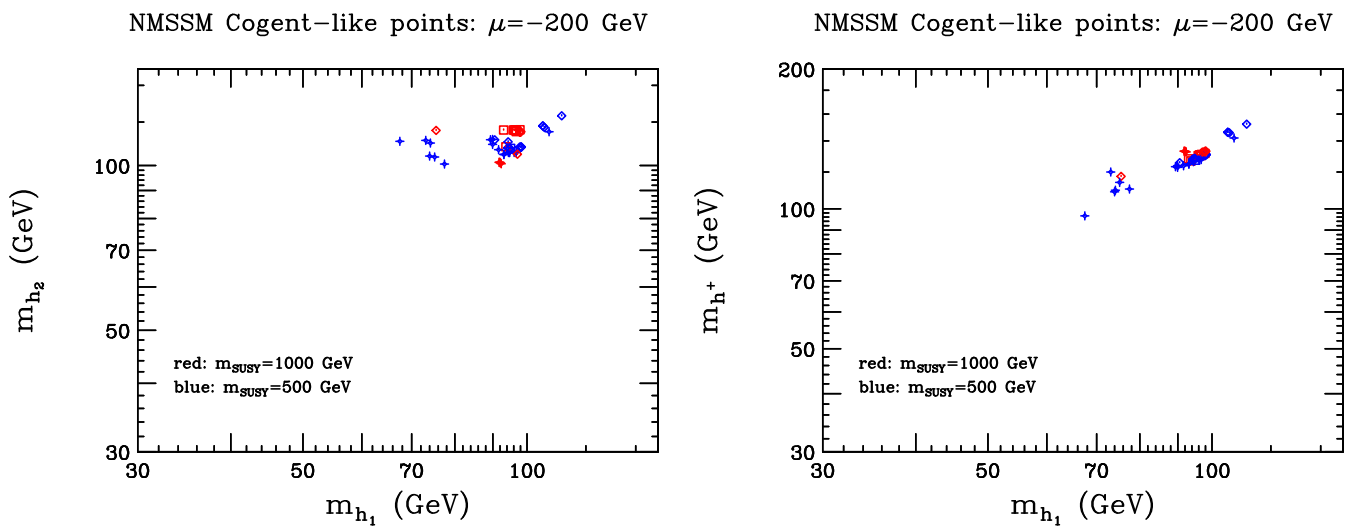

FIG. 3: m_{h_2} and m_{h^+} vs. m_{h_1} for $\mu_{\rm eff} = -200$ points. Parameters not shown are fixed as stated in the text. Only level-I constraints are imposed. There is a lot of point overlap in this plot.

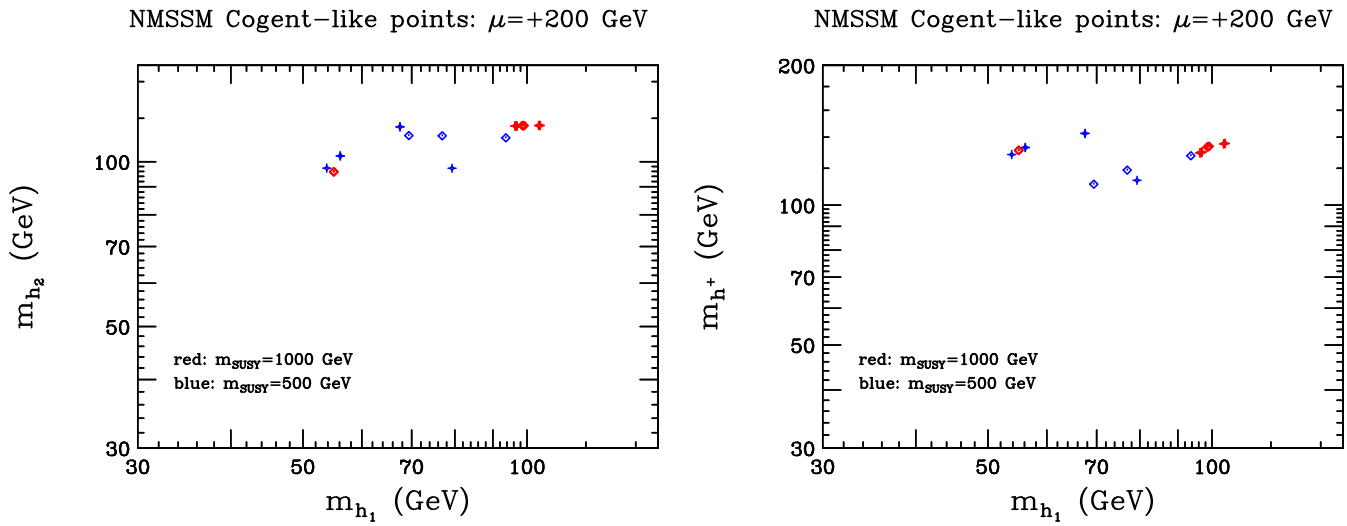

FIG. 4: m_{h_2} and m_{h^+} vs. m_{h_1} for $\mu_{\rm eff} = +200$ points. Parameters not shown are fixed as stated in the text. Only level-I constraints are imposed. There is a great amount of point overlap in this plot.

be seen from the tabulated value of $C_{h_1 b\bar{b}}$. Note that low m_{eff} is achieved despite the fact that the Higgs, namely the h_3, that carries the bulk (74%) of the WW, ZZ coupling-squared has mass $m_{h_3} \sim 126$ GeV. This is because the h_1 carries about 25% of the WW, ZZ coupling-squared and has very low mass.

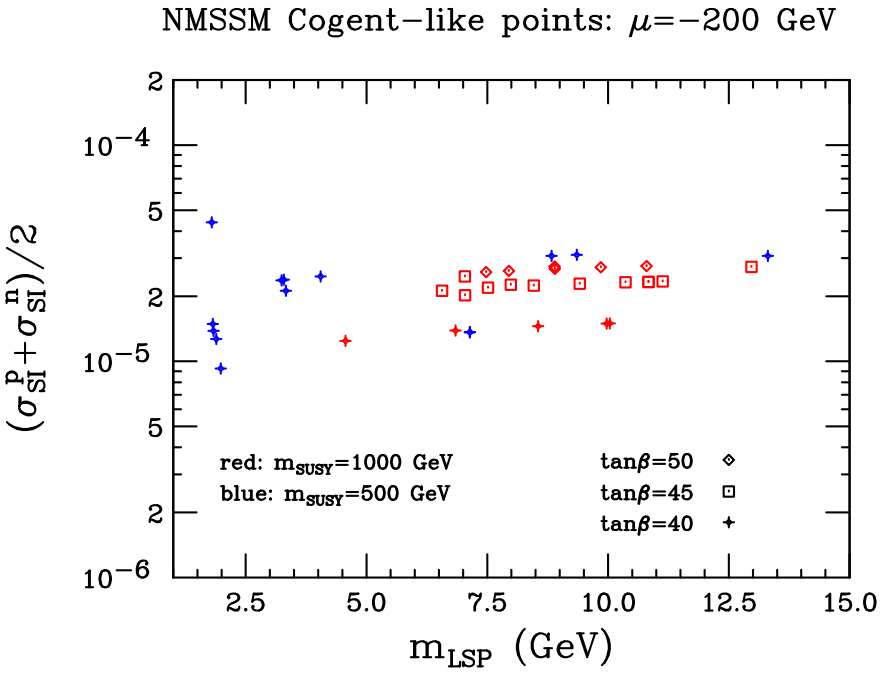

FIG. 5: σ_{SI} vs. $m_{\widetilde{\chi}^0_1}$ for $\mu_{\rm eff} = -200$ GeV points consistent within 1σ (see text) with Tevatron limits on $b\bar{b} + Higgs$ and $t \to h^+ b$. Parameters not shown are fixed as stated in the text. Level-I constraints are imposed.

According to the NMSSMTools package, the only statistically significant Higgs signal for this point in the normal LHC search channels arises in the $WW \to h_3 \to \tau^+\tau^-$ channel where one finds statistical significances relative to background of 3.8 and 14 at low and high luminosity, respectively. Even though the h_3 in this scenario is fairly SM-like ($|C_V(h_3)|^2 \sim 0.72$) its decays to WW, ZZ and $\gamma\gamma$ are suppressed to levels well below those typical of the SM Higgs of the same (low) mass, partly because of the smaller $|C_V(h_3)|^2$ and partly because of significant $h_3 \to Higgs\ pair$ decays. In addition to the $WW \to h_3 \to \tau^+\tau^-$ LHC signal, it seems to us that the $b\bar{b}h_2(\to \tau^+\tau^-)$ signal would also be strong. One would also wish to push discovery of the a_1 in the $gg \to a_1 \to \mu^+\mu^-$ channel — the preliminary estimates of [27] indicate this signal might well be observable given the relatively large value of $C_{a_1 b\bar{b}}$ tabulated above, despite the fact that m_{a_1} is in the Upsilon mass region.

This and other similar points for which h_3 is the SM-like Higgs appear distinctly in Fig. 9. In these scenarios, LEP constraints are easily evaded for the h_1 and h_2 since they have greatly reduced WW, ZZ coupling, and in the case of the h_1 the dominance of $h_1 \to a_1 a_1 \to 4\tau$ decays greatly reduces LEP sensitivity as well. LEP constraints on the h_3 do not enter since $m_{h_3} > 114$ GeV for these cases.

As regards the B physics results in the last row of Table I, the possible range of predictions is that obtained by taking the central prediction of the point after subtracting or adding the theoretical error. These ranges can be compared to the current $\pm 2\sigma$ experimental ranges of Table II. For all but $B(b \to s\gamma)$ there is satisfactory overlap of the predicted range with the experimental range. If we quantify the discrepancy between the predicted and observed ranges as described earlier, the overlap failure is at about the 0.5σ level.

Let us briefly discuss the spin-dependent cross sections for the $\mu = +200$ GeV points. These are basically only a function of $\tan\beta$ and $m_{\widetilde{\chi}^0_1}$. The proton and neutron spin-dependent cross sections are very similar in magnitude. Thus, we confine ourselves to plotting the average value $\sigma_{SD} \equiv (\sigma^p_{SD} + \sigma^n_{SD})/2$ in Fig. 10, even though it is only the separate cross sections that are directly experimentally measurable. One finds that σ_{SD} varies from a low near 0.24×10^{-4} pb for $m_{\widetilde{\chi}^0_1} \sim 2.5$ GeV to a high of $\sim 0.6 \times 10^{-4}$ for $m_{\widetilde{\chi}^0_1} \sim 11$ GeV (the largest value we have considered

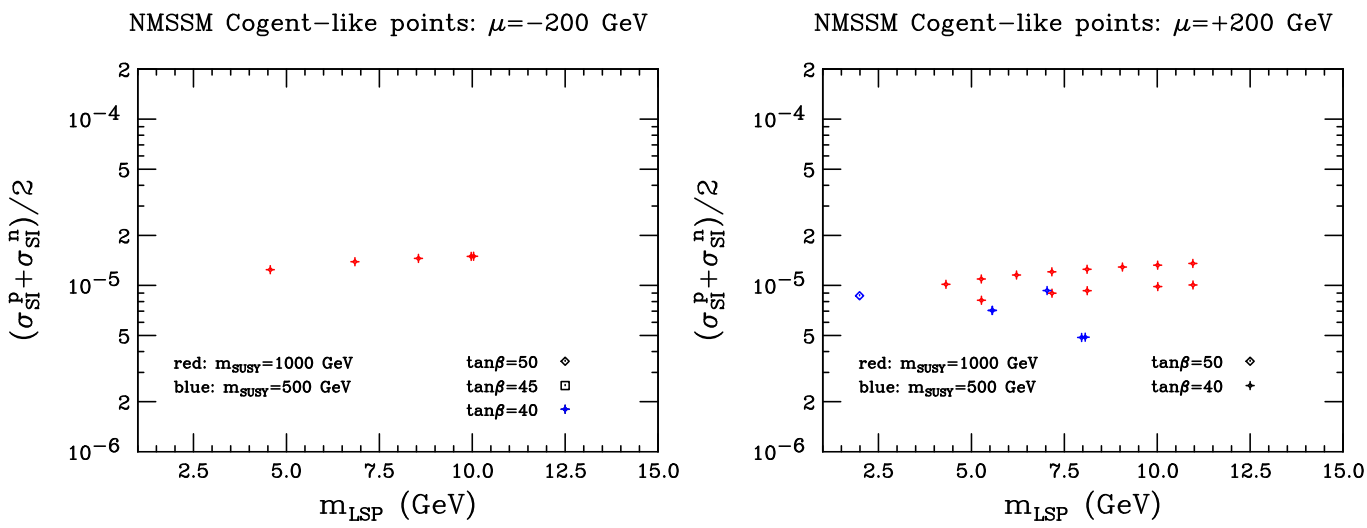

FIG. 6: σ_{SI} vs. $m_{\tilde{\chi}_1^0}$ for points fully consistent with Tevatron limits on $b\bar{b} + Higgs$ and $t \to h^+ b$. Parameters not shown are fixed as stated in the text. Level-I constraints are imposed.

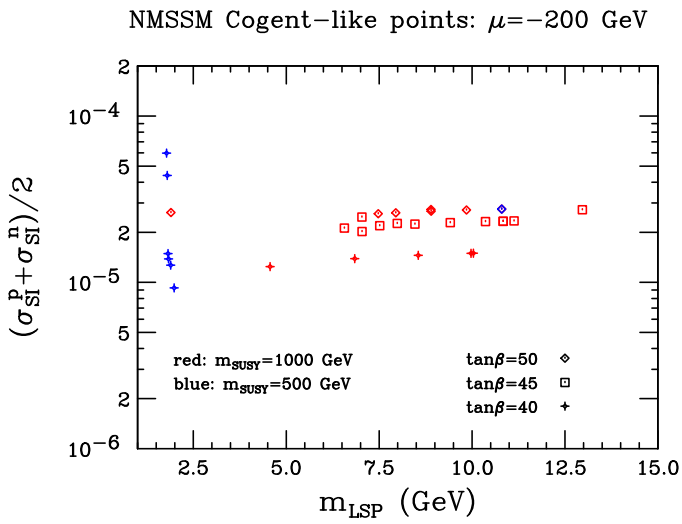

FIG. 7: σ_{SI} vs. $m_{\tilde{\chi}_1^0}$ for $\mu_{\rm eff} = -200$ GeV points satisfying level-I constraints and with $R_\sigma((g-2)_\mu) < 3$. Parameters not shown are fixed as stated in the text.

for $\mu_{\rm eff} = +200$ GeV points).

All the cross section results obtained above are based on the nominal NMSSMTools and micrOMEGAs assumptions. It is worth mentioning several means of enhancing these cross sections. First, we note that the cross section magnitudes

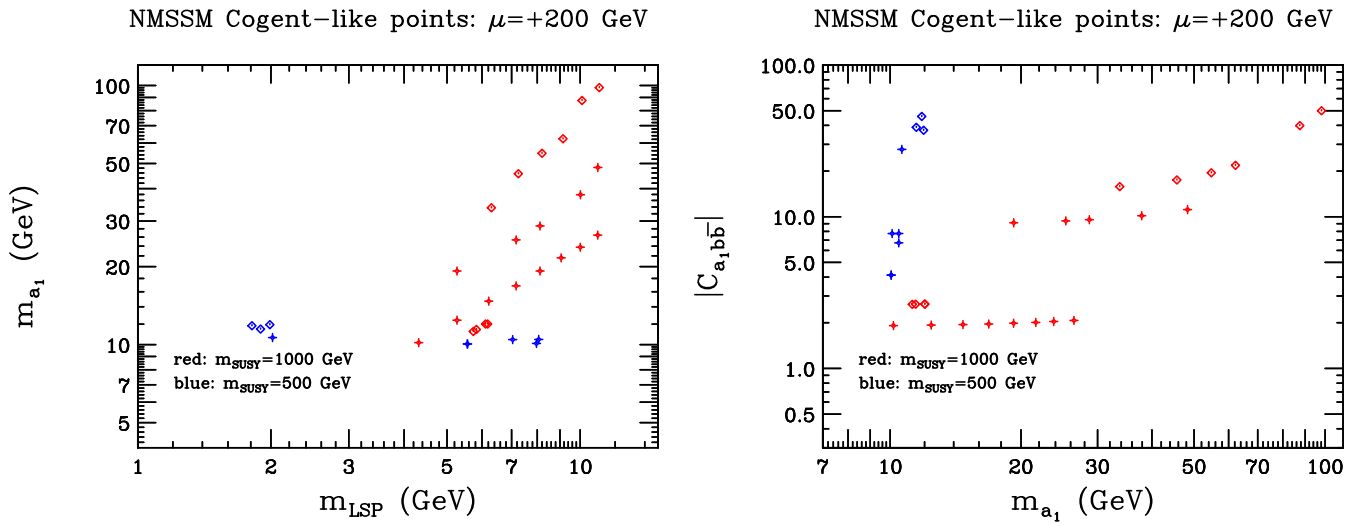

FIG. 8: Left plot: m_{a_1} vs. $m_{\tilde{\chi}_1^0}$ for $\mu_{\rm eff} = +200$ GeV points satisfying level-I constraints. Right plot: $|C_{a_1 b\bar{b}}|$ vs. m_{a_1} for $\mu_{\rm eff} = +200$ GeV points satisfying level-I constraints. Parameters not shown are fixed as stated in the text.

TABLE I: Properties of a particularly attractive but phenomenologically complex NMSSM point with $\mu = +200$ GeV, $\tan\beta = 40$ and $m_{\rm SUSY} = 500$ GeV. This point predicts values for $B(t \to h^+ b) \times B(h^+ \to \tau^+\nu_\tau)$ and for $b\bar{b} + Higgs$ production with $Higgs \to \tau^+\tau^-$ (for all neutral Higgs bosons) below current observed Tevatron limits. In the last row, the brackets give the range of predictions for this point after including theoretical errors as employed in NMHDECAY.

λ	κ	A_λ	A_κ	M_1	M_2	M_3	A_{soft}
0.081	0.01605	−36 GeV	−3.25 GeV	8 GeV	200 GeV	300 GeV	479 GeV

m_{h_1}	m_{h_2}	m_{h_3}	m_{a_1}	m_{a_2}	m_{h^+}
53.8 GeV	97.3 GeV	126.2 GeV	10.5 GeV	98.9 GeV	128.4 GeV

$C_V(h_1)$	$C_V(h_2)$	$C_V(h_3)$	m_{eff}
−0.505	0.137	0.852	101 GeV

$C_{h_1 b\bar{b}}$	$C_{h_2 b\bar{b}}$	$C_{h_3 b\bar{b}}$	$C_{a_1 b\bar{b}}$	$C_{a_2 b\bar{b}}$
0.24	39.7	−5.1	6.7	39.4

$m_{\tilde{\chi}_1^0}$	N_{11}	N_{13}	$m_{\tilde{\chi}_2^0}$	$m_{\tilde{\chi}_1^\pm}$	σ_{SI}	σ_{SD}	Ωh^2
7 GeV	−0.976	−0.212	79.1 GeV	153 GeV	0.93×10^{-5} pb	0.45×10^{-4} pb	0.12

$B(h_1 \to a_1 a_1)$	$B(h_2 \to a_1 a_1)$	$B(h_3 \to Higgs\ pair)$	$B(a_1 \to jj)$	$B(a_1 \to \tau^+\tau^-)$	$B(a_1 \to \mu^+\mu^-)$	$B(a_2 \to \mu^+\mu^-)$
0.96	0.31×10^{-5}	0.3	0.28	0.79	0.003	4.3×10^{-4}

$B(B_s \to \mu^+\mu^-)$	$B(b \to s\gamma)$	$B(h^+ \to \tau^+\nu_\tau)$	$(g-2)_\mu$
$[1.7 - 6.0] \times 10^{-9}$	$[5.8 - 12.5] \times 10^{-4}$	$[0.91 - 4.22] \times 10^{-4}$	$[4.42 - 5.53] \times 10^{-9}$

TABLE II: The $\pm 2\sigma$ experimental ranges for the B physics observables tabulated in the last row of Table I.

$B(B_s \to \mu^+\mu^-)$	$B(b \to s\gamma)$	$B(h^+ \to \tau^+\nu_\tau)$	$(g-2)_\mu$
$< 5.8 \times 10^{-8}$ (95% CL)	$[3.03 - 4.01] \times 10^{-4}$	$[0.34 - 2.3] \times 10^{-4}$	$[0.88 - 4.6] \times 10^{-9}$

have assumed the standard s-quark content for the proton. In [22], the possibility of enhancing σ_{SI} by increasing the s-quark content of the nucleon was discussed. In particular, if one changes the nominal micrOMEGAs values of $\sigma_{\pi N} = 55$ MeV, $\sigma_0 = 35$ MeV to $\sigma_{\pi N} = 73$ MeV, $\sigma_0 = 30$ MeV then σ_{SI} will be enhanced by roughly a factor of 3.3. We believe that such a large shift is not consistent with current constraints and lattice calculations. At most, one might consider $\sigma_{\pi N} \sim 60$ MeV and $\sigma_0 = 30$ MeV [28], leading to an enhancement of about 50%. In fact, the

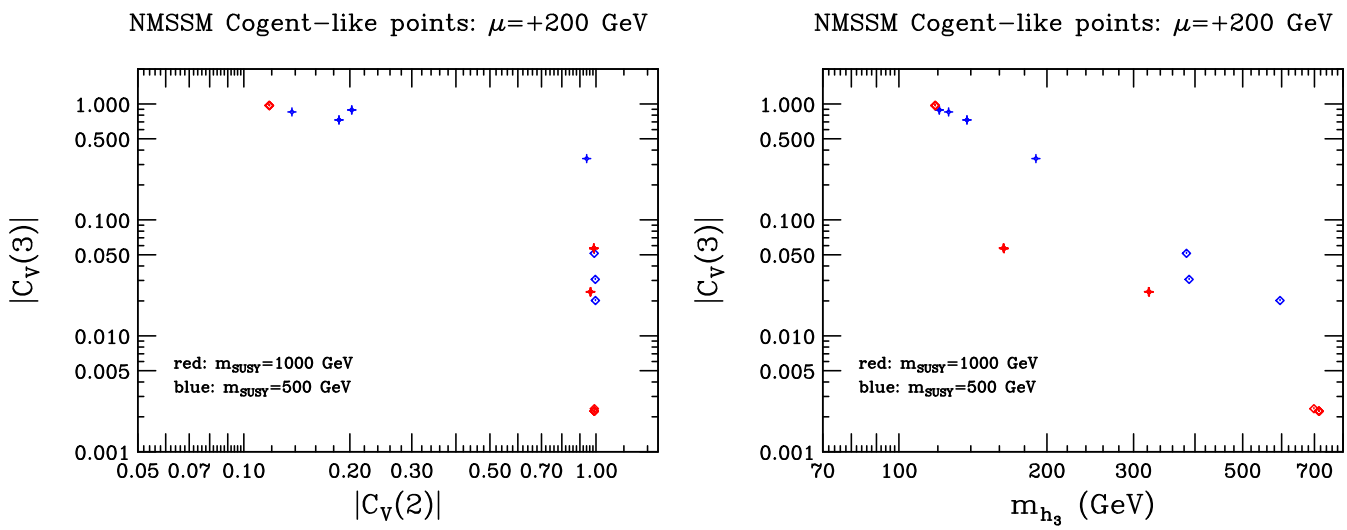

FIG. 9: $|C_V(3)|$ vs. $|C_V(2)|$ and m_{h_3} for $\mu_{\rm eff} = +200$ points. Parameters not shown are fixed as stated in the text. Only level-I constraints are imposed. There is a great amount of point overlap in this plot.

preponderance of information suggests that, if anything, a lower value of $\sigma_{\pi N} \sim 50$ MeV is preferred leading to a decrease in the nucleon's s-quark content and thereby a decrease in σ_{SI}. Another possibility is to employ the larger average local dark matter density $\rho = [0.4 - 0.485]$ GeV/cm^3 suggested in recent papers (see the summary of [11]) instead of the micrOMEGAs default value of 0.3 GeV/cm^3. This would result in a $\sim 60\%$ decrease in the σ_{SI} required to explain the CoGeNT/DAMA events. Using both a 50% s-quark enhancement and the larger ρ one could get about a factor of 2 decrease in the discrepancy between the NMSSM predictions for σ_{SI} and the σ_{SI} values needed to describe the CoGeNT/DAMA observations.

For nominal s-quark content, our results differ somewhat from the NMSSM scan performed in [22]. Their results for σ_{SI} for $\mu_{\rm eff} > 0$ are roughly a factor of 10 below ours. We believe that this is primarily because in their scenarios the h_1 is always SM-like, whereas in our highest-σ_{SI} cases the h_1 has enhanced down-type quark coupling and it is the h_2 or h_3 that is SM-like. This means that their non-SM-like mainly H_d-like Higgs, the h_2 in their case, is typically significantly heavier than in our scenarios. Since $\sigma_{SI} \propto 1/m^4_{H_d-like}$ a factor of 10 increase in σ_{SI} can be achieved if m_{H_d-like} is decreased by a factor of 1.77. For their scans, the largest σ_{SI} is achieved for $m_{H_d-like} \in [205\ {\rm GeV}, 260\ {\rm GeV}]$, whereas our large σ_{SI} values typically have $m_{H_d-like} \leq 100$ GeV. They obtain some gain in cross section since their typical $\mu_{\rm eff}$ is lower (~ 138 GeV vs. our 200 GeV), leading to somewhat larger N^2_{13}. The larger m_{H_d-like} in the scans of [22] imply a larger m_{h^+} with the consequence that their largest σ_{SI} points are within the nominal $\pm 2\sigma$ constraints from $b \to s\gamma$ whereas our high-σ_{SI}, $\mu_{\rm eff} > 0$ points are about 0.5σ outside the $\pm 2\sigma$ region.

VI. SUMMARY AND CONCLUSIONS

We have examined parameter choices within the NMSSM that are potentially capable of yielding a large spin-independent cross section for nucleon-LSP scattering at low LSP mass, consistent with that needed to describe the CoGeNT/DAMA observations. We have required that all LEP and BaBar constraints be satisfied and that accepted points have correct relic density and sufficiently small $B(B_s \to \mu^+\mu^-)$. We have then examined the impact of additional constraints associated with Tevatron observations, other B physics observations and $(g-2)_\mu$.

For standard assumptions regarding the s-quark content of the nucleons, we have found that in the NMSSM the largest spin-independent cross section that can be achieved for a relevant range of $m_{\widetilde{\chi}^0_1}$ if $\mu_{\rm eff} > 0$ is roughly a factor of 10 to 20 shy of that needed to describe the CoGeNT/DAMA event excesses assuming standard relic density, the latter corresponding to $\sigma_{SI} \sim (1.4 - 3.5) \times 10^{-4}$ pb. In particular, σ_{SI} for $\mu_{\rm eff} = +200$ GeV can be no larger

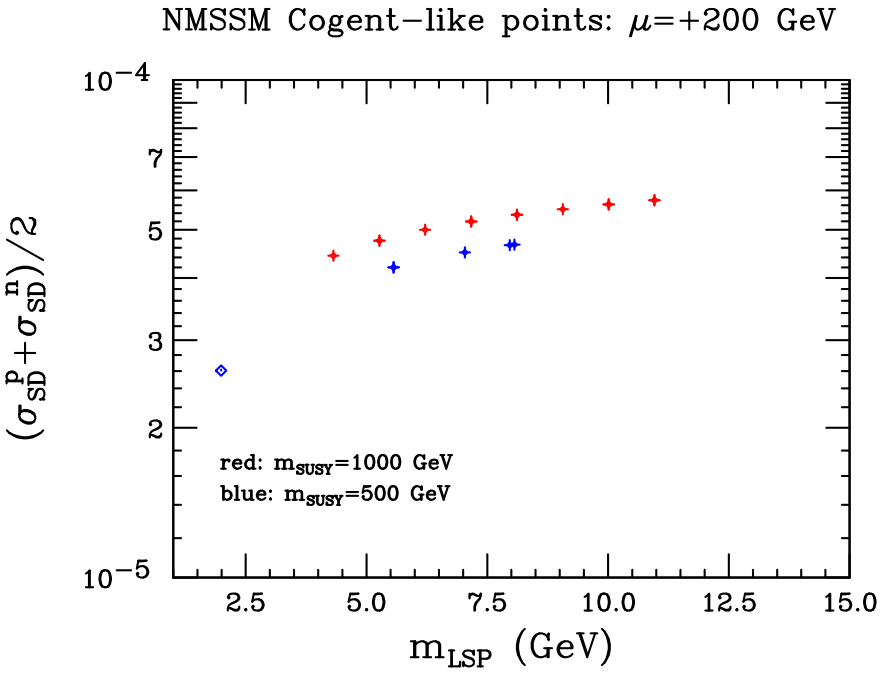

FIG. 10: σ_{SD} vs. $m_{\widetilde{\chi}^0_1}$ for all $\mu_{\rm eff} = +200$ GeV points satisfying level-I constraints.

than 0.14×10^{-4} pb after imposing the Tevatron constraints (but allowing for a very mild violation in $b \to s\gamma$). If one allows for $\rho \sim [0.4 - 0.485]$ GeV/cm^3 instead of 0.3 GeV/cm^3 this will decrease the σ_{SI} required to explain CoGeNT/DAMA by about 60% to perhaps as low as $\sim 10^{-4}$ pb. Nonetheless, our maximal σ_{SI} values, of order 0.14×10^{-4} for $\mu_{\rm eff} = +200$ GeV, would still be well shy of that needed. There is also some uncertainty in the s-quark nucleon content. It is possible to suppose that it could be enhanced by about 50%, although a 50% decrease is perhaps even more reasonable. Combining a 50% increase with the larger ρ, one would still be a factor of at least 5 short of explaining the CoGeNT/DAMA event rates.

For standard s-quark nucleon content, the largest σ_{SI} values found for $\mu_{\rm eff} < 0$ are $\sim 0.6 \times 10^{-4}$ pb, within a factor of 3 to 5 of the needed (assuming nominal $\rho = 0.3$ GeV/cm^3) $\sigma_{SI} = (1.4 - 3.5) \times 10^{-4}$ pb. Unfortunately, $\mu_{\rm eff} < 0$ NMSSM parameter choices yielding such large σ_{SI} all predict an anomalous magnetic moment for the muon that is strongly discrepant with the observed $(g-2)_\mu$. Nonetheless, it is not impossible that there is some resolution of this disagreement coming from physics beyond the NMSSM.

We have illustrated that Tevatron (and, presumably soon, the LHC) constraints on $b\bar{b} + Higgs$ production and $t \to h^+ b$ decays are highly relevant for constraining large-σ_{SI} scenarios. Thus, it is clear that if the CoGeNT observations really are dark matter detection and if the NMSSM is the relevant model, detection of one or more of the a_1, h_1, a_2 and h^+ of the NMSSM at the Tevatron and LHC should be close at hand in the above channels. However, it is also the case that detecting the SM-like Higgs of these scenarios will be very difficult.

On another front, in a companion paper [10] we have demonstrated that allowing an extension of the NMSSM to include additional superpotential terms and/or soft-SUSY-breaking terms (while still keeping just one singlet superfield) will be sufficiently less constraining that σ_{SI} values large enough to describe the CoGeNT excess can be achieved without *any* LEP, Tevatron, BaBar, B-physics (other than a quite small $b \to s\gamma$ deviation) or $(g-2)_\mu$ issues, and using nominal s-quark nucleon content and standard relic density ρ. The key new feature is that the additional parameters allow scenarios consistent with all constraints for which the $\widetilde{\chi}^0_1$ is highly singlet and the h_1 is largely singlet-like with large $\widetilde{\chi}^0_1\widetilde{\chi}^0_1 h_1$ coupling and low m_{h_1}.

Acknowledgements

We would like to thank S. Chang for several helpful conversations. DH is supported by the US Department of Energy, including grant DE-FG02-95ER40896, and by NASA grant NAG5-10842. JFG is supported by US DOE grant DE-FG03-91ER40674. JFG and DH also received support from the Aspen Center for Physics while working on this project.

Bibliography

[1] C. E. Aalseth *et al.* [The CoGeNT Collaboration], arXiv:1002.4703 [astro-ph.CO].
[2] A. L. Fitzpatrick, D. Hooper and K. M. Zurek, arXiv:1003.0014 [hep-ph].
[3] J. Kopp, T. Schwetz and J. Zupan, JCAP **1002**, 014 (2010) [arXiv:0912.4264 [hep-ph]].
[4] S. Chang, J. Liu, A. Pierce, N. Weiner and I. Yavin, arXiv:1004.0697 [hep-ph].
[5] R. Bernabei *et al.*, arXiv:1002.1028 [astro-ph.GA].
[6] D. Hooper, J. I. Collar, J. Hall and D. McKinsey, arXiv:1007.1005 [hep-ph].
[7] E. Kuflik, A. Pierce and K. M. Zurek, arXiv:1003.0682 [hep-ph].
[8] D. Feldman, Z. Liu and P. Nath, arXiv:1003.0437 [hep-ph].
[9] D. Hooper and T. Plehn, Phys. Lett. B **562**, 18 (2003) [arXiv:hep-ph/0212226]; A. Bottino, N. Fornengo and S. Scopel, Phys. Rev. D **67**, 063519 (2003) [arXiv:hep-ph/0212379].
[10] A. V. Belikov, J. F. Gunion, D. Hooper and T. M. P. Tait, arXiv:1009.0549 [hep-ph].
[11] M. Pato, O. Agertz, G. Bertone, B. Moore and R. Teyssier, Phys. Rev. D **82**, 023531 (2010) [arXiv:1006.1322 [astro-ph.HE]].
[12] E. Komatsu *et al.* [WMAP Collaboration], Astrophys. J. Suppl. **180**, 330 (2009) [arXiv:0803.0547 [astro-ph]].
[13] J. R. Ellis, J. F. Gunion, H. E. Haber, L. Roszkowski and F. Zwirner, Phys. Rev. D **39**, 844 (1989); H. P. Nilles, M. Srednicki and D. Wyler, Phys. Lett. B **120**, 346 (1983); J. E. Kim and H. P. Nilles, Phys. Lett. B **138**, 150 (1984); M. Drees, Int. J. Mod. Phys. A **4**, 3635 (1989).
[14] R. Dermisek and J. F. Gunion, Phys. Rev. Lett. **95**, 041801 (2005) [arXiv:hep-ph/0502105].
[15] J. R. Espinosa and M. Quiros, Phys. Lett. B **305**, 98 (1993) [arXiv:hep-ph/9301285]; K. Funakubo, S. Tao and F. Toyoda, Prog. Theor. Phys. **109**, 415 (2003) [arXiv:hep-ph/0211238].
[16] R. Dermisek and J. F. Gunion, Phys. Rev. D **75**, 075019 (2007) [arXiv:hep-ph/0611142].
[17] J. F. Gunion, D. Hooper and B. McElrath, Phys. Rev. D **73**, 015011 (2006) [arXiv:hep-ph/0509024];
[18] U. Ellwanger, J. F. Gunion and C. Hugonie, JHEP **0502**, 066 (2005) [arXiv:hep-ph/0406215].
[19] U. Ellwanger and C. Hugonie, Comput. Phys. Commun. **175**, 290 (2006) [arXiv:hep-ph/0508022].
[20] G. Belanger, F. Boudjema, A. Pukhov and A. Semenov, Comput. Phys. Commun. **176**, 367 (2007) [arXiv:hep-ph/0607059].
[21] U. Ellwanger and C. Hugonie, http://www.th.u-psud.fr/NMHDECAY/nmssmtools.html.
[22] D. Das and U. Ellwanger, arXiv:1007.1151 [hep-ph].
[23] S. Schael *et al.* [ALEPH Collaboration], JHEP **1005**, 049 (2010) [arXiv:1003.0705 [hep-ex]].
[24] D. Benjamin *et al.* [Tevatron New Phenomena & Higgs Working Group], arXiv:1003.3363 [hep-ex].
[25] V. M. Abazov *et al.* [D0 Collaboration], Phys. Lett. B **682**, 278 (2009) [arXiv:0908.1811 [hep-ex]].
[26] R. Dermisek and J. F. Gunion, Phys. Rev. D **81**, 075003 (2010) [arXiv:1002.1971 [hep-ph]].
[27] R. Dermisek and J. F. Gunion, Phys. Rev. D **81**, 055001 (2010) [arXiv:0911.2460 [hep-ph]].
[28] We wish to thank H. Leutwyler for very useful communications regarding these issues.